BMC Immunology

RESEARCH

Open Access

Macrophage-targeted anti-CCL2 immunotherapy enhances tumor sensitivity to 5-fluorouracil in a Balb/c-CT26 murine colon carcinoma model measured using diffuse reflectance spectroscopy

Shelby N. Bess, Gage J. Greening, Narasimhan Rajaram and Timothy J. Muldoon*

Abstract

Background: Immunotherapy in colorectal cancer (CRC) regulates specific immune checkpoints and, when used in combination with chemotherapy, can improve patient prognosis. One specific immune checkpoint is the recruitment of circulating monocytes that differentiate into tumor-associated macrophages (TAMs) and promote tumor angiogenesis. Changes in vascularization can be non-invasively assessed via diffuse reflectance spectroscopy using hemoglobin concentrations and oxygenation in a localized tumor volume. In this study, we examine whether blockade of monocyte recruitment via CCL2 (macrophage chemoattractant protein-1) leads to enhanced sensitivity of 5-fluorouracil (5-FU) in a CT26-Balb/c mouse model of CRC. It was hypothesized that the blockade of TAMs will alter tumor perfusion, increasing chemotherapy response. A subcutaneous tumor model using Balb/c mice injected with CT26 colon carcinoma cells received either a saline or isotype control, anti-CCL2, 5-FU, or a combination of anti-CCL2 and 5-FU.

Results: Findings show that 12 days post-treatment, monocyte recruitment was significantly reduced by approximately 61% in the combination group. This shows that the addition of anti-CCL2 to 5-FU slowed the fold-change (change from the original measurement to the final measurement) in tumor volume from Day 0 to Day 12 (~5 fold). Modest improvements in oxygen saturation (~30%) were observed in the combination group.

Conclusion: The findings in this work suggest that the blockade of CCL2 is sufficient in the reduction of TAMs that are recruited into the tumor microenvironment and has the ability to modestly alter tumor perfusion during early-tumor response to treatment even though the overall benefit is relatively modest.

Keywords: Colorectal cancer, Tumor-associated macrophages, Diffuse reflectance spectroscopy, Immunomodulation

Introduction

Colorectal cancer (CRC) is estimated to account for 149,500 new cancer cases annually in the United States, making it the 4th most common cancer type overall (behind breast, prostate, and lung), and resulting in 52,980 annual deaths [1]. Locally-advanced CRC (stages II-III), which accounts for approximately 20% of cases, describes cancer that has spread from the site of the primary tumor to surrounding tissue or lymph nodes but has not metastasized [2–4]. The standard of treatment for locally-advanced CRC is neoadjuvant chemo-radiotherapy (CRT) using 5-fluorouracil (5-FU), followed

*Correspondence: tmuldoon@uark.edu
Department of Biomedical Engineering, University of Arkansas, 1 University of Arkansas, Fayetteville, AR 72701, USA

by total mesorectal excision (TME) surgery [5]. Following neoadjuvant CRT, biopsies are examined to determine pathologic response. Ideally, patients will exhibit pathologic complete response (pCR) when there is an absence of residual cancer cells in a histological examination. Patients achieving pCR have a reduced risk of distal recurrence [2]. However, pCR is achieved in less than 30% of cases, resulting in distal recurrence rates of 25%, which is the primary cause of CRC-related death [2]. Thus, the development of more effective treatments for CRC is in urgent need. An emerging strategy called immunomodulation therapy, or immunotherapy, has gained clinical momentum in recent years to aid neoadjuvant CRT in reducing tumor burden and recurrence risk [6–8].

Immunotherapy in CRC is a broad approach aimed at modulating the immune system to inhibit checkpoints of pro-tumor pathways to increase tumor sensitivity to chemotherapy [6]. One specific immunotherapy strategy is the blockade of CCL2/MCP-1 (monocyte chemoattractant protein-1), an elevated cytokine during CRC progression which recruits monocytes to the tumor microenvironment [9]. Monocytes differentiate into tumor-associated macrophages (TAMs), which have pro-tumor functions in CRC [10–19], although conflicting studies have reported anti-tumor functions of TAMs at tumor margins [20–23]. Pro-tumor functions of TAMs include direct secretion of angiogenic growth factors (GFs) leading to an increase in vascular endothelial growth factor (VEGF) [10, 19, 24] and ECM-degrading matrix metalloproteases (MMPs) which allow for the release of ECM-sequestered angiogenic GFs [10, 17]. FDA approval of anti-VEGFs, such as bevacizumab, has shown significant benefit in overall survival in breast cancer; however, it has shown no significant benefit in terms of overall survival, leading to many clinicians restricting its use and a shift in focus to modulation of cytokines [25]. CCL2-mediated TAM infiltration is linked to increased inflammation, angiogenesis, and tumorigenesis; therefore, anti-CCL2 immunotherapy has the potential to reduce tumor burden and recurrence risk [12, 26].

Recent research has explored CCL2 blockade as an immunotherapy strategy in various mouse models. Popivanova et al. showed that CCL2 blockade reduced neovascularization and colon tumor size in Balb/c mice [27]. Zhu et al. showed that administration of anti-CCL2 in combination with temozolomide chemotherapy in C57BL/6 mice with GL261 glioma significantly prolonged survival [28]. Svensson et al. demonstrated that CCL2 blockade in FVB/N mice with MCF-7 breast cancer decreased TAM infiltration and reduced estrogen-stimulated cancer growth [29]. Kirk et al. showed that delivering anti-CCL2 in combination with docetaxel chemotherapy in SCID mice with C4-2B prostate adenocarcinoma inhibited tumor progression [30].

It has been shown that TAMs not only have a role in tumor progression, but also in cancer chemoresistance. Zhang et al. demonstrated that TAMs directly contribute to 5-FU chemoresistance in CRC and concluded that TAM pathways (such as CCL2) were potential immunotherapy targets to increase the efficacy of 5-FU chemotherapy [13]. Although studies have investigated the use of a CCL2 antagonist on the recruitment of macrophages and their interactions between other immune cells, no studies have correlated macrophage recruitment to the functional changes in the tumor microenvironment (i.e., hypoxia).

This study further examines the role of the CCL2/MCP-1 axis in colorectal cancer via antibody mediated blockade of CCL2 combined with 5-FU chemotherapy in Balb/c mice with subcutaneous CT26 colon carcinoma allografts. Mice were separated into five groups: saline control, isotype control. anti-CCL2 immunotherapy, 5-FU chemotherapy, or combination therapy groups. 5-FU was expected to alter tumor hemodynamics due to a rapid decrease in cellular metabolism leading to a decrease in oxyhemoglobin conversion to deoxyhemoglobin. The addition of anti-CCL2 was expected to modulate this effect. Through the duration of the study, tumor perfusion in vivo was longitudinally measured via DRS to quantify perfusion metrics such as tissue hemoglobin content (THC) and tissue oxygen saturation (StO_2). DRS measurements were correlated to end-point immunohistochemistry (IHC) markers of hypoxia (carbonic anhydrase-9) and microvasculature (CD31), along with tumor-associated macrophage recruitment (CD68) and M2 tumor-associated macrophage recruitment (CD163). This study examines one major hypothesis: CCL2 blockade in the tumor microenvironment increases the sensitivity of CT26 tumors to 5-FU chemotherapy, which is quantified via longitudinal tumor growth, DRS-derived metrics and IHC analysis.

Materials and methods

Cell line

CT26 (ATCC®, CRL-2638™) cells were maintained under standard conditions in Roswell Park Memorial Institute (RPMI)-1640 medium (ATCC®, 30–2001™) supplemented with 10% fetal bovine serum (ATCC®, 30–2020), 1% antibiotic antimycotic solution (Sigma-Aldrich, A5955-100ML), and 0.2% amphotericin B/gentamicin (Thermo Fisher Scientific, R015010). CT26 cells were brought to the third passage for a total of approximately 5×10^6 cells prior to implantation.

Animal model

All animal experiments were approved by the University of Arkansas Institutional Animal Care and Use Committee (IACUC #18060 and #21014) and carried out in accordance with the National Institutes of Health Guide for the Care and Use of Laboratory Animals and the ARRIVE guidelines. All efforts were made to minimize animal suffering and to reduce the number of mice used. Nine-week-old female Balb/c mice (n = 95) were obtained from The Jackson Laboratory (Bar Harbor, ME, USA). Upon arrival, mice were housed in groups of three at 23 °C ± 1 °C and 50% ± 10% humidity with a 12:12-h light–dark cycle and had access to water and standard rodent food ad libitum. Mice underwent one week of environmental acclimation, including daily handling (1 min per mouse) for stress adaptation to future handling during measurements. Five days after arrival, hair on the injection site (left flank) was removed via shaving and a depilatory lotion, and then cleaned. Seven days after arrival, the mice underwent subcutaneous (SQ) injection of 1×10^6 CT26 cells into the left flank. Tumors were allowed to grow until they reached 75 ± 5 mm^3 (day 0), as measured via $V = \left(L \cdot W^2\right)/2$, which took an average of 10 ± 4 days.

Control and experimental groups

Balb/c mice were randomly divided into five groups once tumors reached 75 mm^3. The first group (n = 16) received saline injections as a control. The second group (n = 15) received an isotype control. The third group received anti-CCL2 only (n = 14). The fourth group (n = 14) received 5-FU only. The fifth group (n = 13) received a combination of 5-FU and anti-CCL2. Mice were euthanized via cervical dislocation if they reached humane end-point euthanasia criteria as specified by the University of Arkansas IACUC (maximum tumor diameter ≥ 20 mm, body condition score ≤ 2, weight loss ≥ 20% from baseline, macroscopic evidence of ulceration or chronic pain or distress detailed by the University of Rhode Island IACUC.

Chemotherapy

5-Fluorouracil (5-FU), purchased from Sigma-Aldrich (St. Louis, MO, USA), is an antitumor chemotherapy agent that induces p53-dependent apoptosis and decreases proliferation [31]. 5-FU powder (Sigma Aldrich, #F6627-10G) was diluted in DMSO at 40 mg/mL and stored at − 20 °C for a maximum of two months before injection. A second dilution of 5-FU/DMSO was created in sterile saline (VWR, Radnor, PA, #89167-774) to bring the 5-FU concentration to 20 mg/mL. On the day of injection, aliquots of 20 mg/mL 5-FU + DMSO in sterile saline were further diluted to 3 mg/mL 5-FU/saline in sterile microcentrifuge tubes (VWR, #20,170–038), and brought to 37.3 °C. Using a 28G insulin syringe (VWR, #BD329410), mice in the 5-FU and combination groups received daily intraperitoneal (IP) administration of 5-FU at a concentration of 15 mg/kg/dose [32] until day 10 (165 mg/kg/week). This resulted in an average injection of 300 µg 5-FU in 100 µL vehicle, based on average mouse weight of approximately 20 g at the time of injection.

Immunotherapy

Anti-CCL2 (clone number: 2H5), purchased from Bio X Cell (West Lebanon, NH, USA), is a monoclonal antibody that neutralizes murine CCL2 [31, 33]. Anti-CCL2 (Bio X Cell, 2H5, #BE0185) was shipped at 7.4 mg/mL in PBS and stored at 4 °C before injection. On the day of injection, aliquots of 7.4 mg/mL anti-CCL2/PBS solution were diluted with sterile saline (VWR, #89167-774) to 1 mg/mL anti-CCL2/saline in sterile microcentrifuge tubes (VWR, #20170-038), and brought to 37.3 °C. Using a 28G insulin syringe (VWR, #BD329410), anti-CCL2 and combination groups received IP administration of anti-CCL2 at a concentration of 4.0 mg/kg/dose [28, 31] given every other day through day 10 (24 mg/kg/week). This resulted in an average injection of 80 µg anti-CCL2 (2H5) in 100 µL vehicle, based on average mouse weight of 20 g at the time of injection.

Isotype control

An Armenian hamster IgG isotype control, purchased from Bio X Cell (West Lebanon, NH, USA), is a polyclonal antibody that is ideal for its use as a non-reactive control. The isotype control (IgG) (Bio X Cell, #BE0091) was shipped at 7.4 mg/mL in PBS and stored at 4 °C before injection. On the day of injection, aliquots of 7.4 mg/mL IgG/PBS solution were diluted with sterile saline (VWR, #89167-774) to 1 mg/mL IgG/saline in sterile microcentrifuge tubes (VWR, #20170-038), and brought to 37.3 °C. Using a 28G insulin syringe (VWR, #BD329410), the isotype group received IP administration of IgG at a concentration of 4.0 mg/kg/dose [28, 31] given every other day through day 10 (24 mg/kg/week). This resulted in an average injection of 80 µg IgG in 100 µL vehicle, based on average mouse weight of 20 g at the time of injection.

Diffuse reflectance spectroscopy

DRS instrumentation

The DRS probe (FiberTech Optica, Kitchener, ON, Canada) was 1.0 m in total length, with the split position located 0.67 m from the common (distal) end. Five

individual optical fibers (one source and four detectors) were integrated within the distal brass ferrule (6.35 mm diameter × 50 mm long). All fibers were arranged linearly in a slit line, resulting in source-detector separations (SDS) of 0.75, 2.00, 3.00, and 4.00 mm. Each multimodal optical fiber consisted of a high-OH silica core, a silica cladding, and a polyimide jacket optimized for a wavelength range of 190–1200 nm, which exceeded the desired wavelength range of 450–750 nm used in this study. The source fiber, as well as the 2.00, 3.00, and 4.00 SDS fibers (FiberTech Optica, SUV400/440PI) consisted of a 400/440 µm ± 2% silica core/cladding with a 470 µm ± 5% polyimide jacket. The 0.75 mm SDS fiber (FiberTech Optica, SUV200/220PI) consisted of a 200/220 µm ± 2% silica core/cladding with a 245 µm ± 5% polyimide jacket. These optical fibers were included to sample into the subcutaneous murine CT26 tumor at multiple sampling depths to quantify THC, StO_2, and HbO_2, and dHb. A 20 W tungsten-halogen lamp (Ocean Optics, HL-2000-HP) provided broadband light (360–2400 nm) to the 400 µm core source fiber. A spectrometer (Ocean Optics, FLAME-S) with a Sony ILX511B linear silicon CCD array (2,048-pixel elements) collected diffusely reflected light from the 3 mm SDS (Fig. 1).

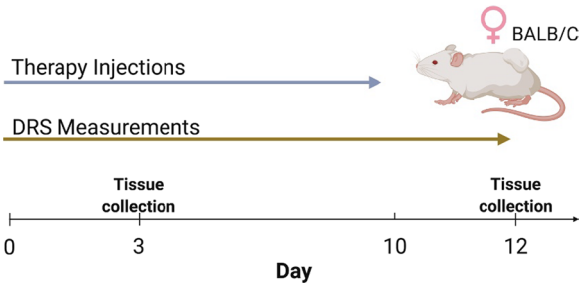

Fig. 2 Timeline for study. Daily DRS measurements were taken after tumor volumes reached 75 mm^3 up until endpoint analysis (Day 3 or 12). Therapy injections were given on days 0 to 10. 5-FU treated mice were given daily injections while the other treatment groups (saline and isotype controls and anti-CCL2) were given injections every other day. The combination group followed the treatment schedule of the anti-CCL2 and 5-FU groups. Figure was created with BioRender.com

Diffuse reflectance spectroscopy measurements

All mice (n = 95) underwent DRS measurements starting at day 0. The hair on the tumor site was removed via depilatory lotion and then cleaned 24 h prior to the first DRS measurement. In this study, only the 3.00 mm SDS was used. The 3.00 mm SDS provided an optimal balance of signal-to-noise (> 15 dB), appropriate in vivo integration time (70 ms), and wavelength-dependent sampling depth (~ 1.3 to 2.1 mm). DRS measurements were taken daily until the mice reach endpoint IHC analysis (Fig. 2).

The DRS probe was placed on the tumor such that the linear arrangement of optical fibers was collinear with the long axis of the tumor (cranial to caudal direction) of non-anesthetized mice while spectra were collected. For each tumor, ≥ 20 DRS measurements were acquired at an integration time of 70 ms. Day-to-day fluctuations in light source intensity were controlled by calibration with a Spectralon® 20% diffuse reflectance standard. Daily spectrometer dark noise was subtracted from each spectra.

Each DRS measurement resulted in a value for THC, StO_2, HbO_2, dHb (630 nm) [34], and a chi-square (χ^2) value. THC, StO_2, HbO_2, dHb were quantified by inputting raw DRS spectra into custom lookup-table (LUT)-based MATLAB software with a priori values for oxygenated and deoxygenated hemoglobin extinction coefficients [35–37]. The software performed an iterative model fit (1×10^4 iterations) to the raw DRS data to quantify THC, StO_2, HbO_2, dHb. The χ^2 value indicated goodness-of-fit between the model fit and raw DRS data; high χ^2 values usually implied specular reflection due to

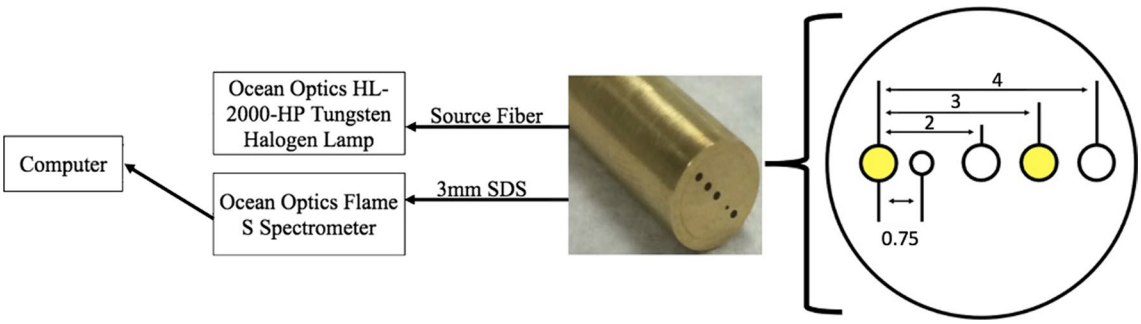

Fig. 1 Schematic of DRS system. The DRS probe was connected to an Ocean Optics Flame S spectrometer through the 3 mm SDS and to an Ocean Optics HL-2000-HP Tungsten Halogen Lamp through the source fiber. The halogen lamp and spectrometer were connected to a computer display with a custom LABView software program to collect spectra and calibration measurements

user movement. Therefore, if χ^2 of the spectra exceeded 10, data were discarded. THC, StO_2, HbO_2, dHb values were averaged to yield a daily result.

Immunohistochemistry and quantification

Tumors were placed in a 50 mL conical centrifuge tube of 10% neutral buffered formalin for 24 h at 4 °C. After 24 h, formalin was replaced with 50 mL phosphate-buffered saline (PBS), then placed in 50 mL 70% ethanol before shipment (IHC World, Ellicott City, MD, USA) for IHC staining. Tumors were paraffin-embedded, sectioned in 5 μm sections, and stained for anti-CD68 (Abcam®, ab125212), anti-CD163 (Abcam®, ab182422), anti-carbonic anhydrase-9 (CA-IX) (Abcam®, ab184006), anti-CD31 (Abcam®, ab28364), and H&E.

Total-tumor-associated macrophage recruitment

anti-CD68 stained slides were imaged with a wide-field upright microscope (Nikon, Eclipse Ci), with a 40X/1.30NA oil objective lens (Nikon, CFI Plan Fluor 60X), digital camera (Nikon, DS-Fi2), and PC-based camera control unit (Nikon, DS-U3). For each mouse, three 5 μm tissue sections were imaged and nine high-powered fields-of-view (FOV: 50 μm^2) were taken for each of the three sections for a total of nine TAM FOVs per tumor. In ImageJ, images were converted to 8-bit and thresholded using the average pixel intensity of a positively stained TAM using Otsu's method. All counts were made blinded to DRS data. All positively stained cells were counted over the nine FOVs to calculate the average TAM count per FOV.

M2-tumor-associated macrophage recruitment

anti-CD163 stained slides were imaged with a wide-field upright microscope (Nikon, Eclipse Ci), with a 40X/1.30NA oil objective lens (Nikon, CFI Plan Fluor 60X), digital camera (Nikon, DS-Fi2), and PC-based camera control unit (Nikon, DS-U3). For each tumor, three 5 μm tissue sections were imaged and three high-powered fields-of-view (FOV: 50 μm^2) were taken for each of the three sections for a total of nine TAM FOVs per tumor. In ImageJ, images were converted to 8-bit and the color channels were separated (brown vs blue). Images containing the positive brown staining were thresholded using the average pixel intensity of a positively stained TAM using Otsu's method. All counts were made blinded to DRS data. All positively stained cells were counted over the nine FOVs to calculate the average TAM count per FOV.

Hypoxia

Slides stained for anti-CA-IX were imaged with a wide-field upright microscope (Nikon, Eclipse Ci), 10X/0.3NA objective lens (Nikon, CFI Plan Fluor 10X), digital camera (Nikon, DS-Fi2), and PC-based camera control unit (Nikon, DS-U3) [38]. For each tumor, three 5 μm thick tissue sections were imaged. Three high-powered fields-of-view (FOV: 200 μm^2) were taken for each of the three sections for a total of nine FOVs per tumor. In ImageJ, images were thresholded using "Color Threshold" based on the darkest pixel color (brown). The hypoxic area for each image was calculated using this formula:

$$\text{Hypoxic area} = \frac{\text{Positive CA} - \text{IX stained area}(\text{pixels})}{\text{Total area}\,(\text{pixels})} \times 100\%$$

where the numerator represents the total number of pixels that were captured using the "Color Threshold" and the denominator represents the total number of pixels within the image. All positively stained areas were counted over the nine FOVs to calculate the average hypoxic area.

Vasculature

Slides stained for anti-CD31 were imaged with a wide-field upright microscope (Nikon, Eclipse Ci), 10X/0.3NA objective lens (Nikon, CFI Plan Fluor 10X), digital camera (Nikon, DS-Fi2), and PC-based camera control unit (Nikon, DS-U3). For each tumor, three 5 μm thick tissue sections were imaged. Three high-powered fields-of-view (FOV: 200 μm^2) were taken for each of the three sections for a total of nine FOVs per tumor. In ImageJ, images were thresholded using "Color Threshold" based on the darkest pixel color (brown). The vascular density for each image was calculated using this formula [39]:

$$\text{Vascular Density} = \frac{\text{Positive } CD31 \text{ stained area}(\text{pixels})}{\text{Total area}(\text{pixels})} \times 100\%$$

where the numerator represents the total number of pixels that were captured using the "Color Threshold" and the denominator represents the total number of pixels within the image. All positively stained areas were counted over the nine FOVs to calculate the average vascular density.

Statistical analysis

The significance of datasets was set to $p < 0.05$. Statistical analysis was performed using Prism (GraphPad, version 8.4.3 (471)). A mixed-effects model with a Dunnett's multiple comparisons test was used to assess statistical differences for the tumor volume and DRS data. Simple linear regression was used to determine the goodness of fit for the correlation plots.

Results

Combination therapy shows improvement in tumor volume survival and slows tumor growth

To study the effects of combinatorial therapy, tumor volumes were compared between each experimental group. Tumor volumes were measured daily after the initial threshold of 75 mm^3 was reached. Figure 3A shows representative images of resected tumors and H&E-stained tumors for each group. These results suggest that the addition of anti-CCL2 to 5-FU decreases tumor volume over time. In Fig. 3B–E., the average fold-change in tumor volume between groups was explored during our twelve-day study. The isotype and saline controls show a similar fold change in tumor volume across the duration of treatment. In the anti-CCL2 group, there was a smaller fold change in tumor volume with one significant difference observed on Day 6 ($p=0.0089$). The 5-FU showed a smaller fold change in tumor volume than the control groups and the anti-CCL2 group. Significant differences were observed on Days 5 through 12 with greatest difference in fold change in tumor volume observed on Day 5 ($p=0.0003$) when compared to the saline control. The combination group showed the greatest difference in the average fold change in tumor volume during the course of treatment, with exception to Days 10 and 12. The greatest difference in the fold change in tumor volume between the saline group and the combination group was seen on Day 6 ($p<0.0001$). This trend between these two groups continues through the duration of the study. Overall, throughout the duration of the study, the combination therapy showed aa approximately one to two-fold change (change from the original measurement to the final measurement) decrease in tumor growth.

Anti-CCL2 significantly reduces TAM recruitment into the tumor microenvironment

To test the effect of anti-CCL2 on TAM recruitment, subcutaneous tumors were labeled with a pan-TAM marker, CD68. When comparing the macrophage recruitment between groups, the combination group showed the greatest decrease in TAMs between days three and twelve (Fig. 4A, C). For the saline and isotype controls, both groups showed similar results for total macrophage recruitment for both days 3 and 12. While imaging the isotype group on day 12, the intensity of the brown pixels (CD68 marker) was fainter than that of the saline control. The intensity of these pixels did not affect the overall result for total macrophage recruitment. After three days of treatment, the control groups showed similar results while the anti-CCL2 group showed a modest decrease (~10%) in total TAM recruitment. When compared to the saline control, the 5-FU group showed a decrease of ~20% in total TAM recruitment with a significant difference when compared to the saline control ($p=0.0159$) while the combination group showed a major decrease in total TAM recruitment (~25%) with a significant difference when compared to the saline control ($p=0.0003$). On day twelve, again, the controls showed similar results while the anti-CCL2, 5-FU, and combination groups showed a significant difference ($p<0.0001$ for all groups). The anti-CCL2 showed an ~20% decrease in total TAM recruitment from day three to twelve. The 5-FU group showed an ~15% decrease in total TAM recruitment from day three to twelve. Finally, the combination group showed an ~20% decrease in total TAM recruitment from day three to twelve. Overall, results show that the addition of anti-CCL2 to 5-FU shows a significant decrease in total TAM recruitment into the microenvironment.

Since TAM infiltration increases pro-tumor functions such as angiogenesis and tumor burden, we wanted to look at the recruitment of M2-phenotype TAMs into the tumor microenvironment using CD163 (a common M2 marker). Similar to the results shown in Fig. 4A, the combination group shows the greatest decrease in the recruitment of M2 TAMs. Significant differences in M2 TAM infiltration were observed in the treatment groups on days three and twelve when compared to the saline control (Fig. 4B, D). On day 3, anti-CCL2 treated tumors showed a modest decrease (~20%) in M2 TAMs ($p=0.004$), while the 5-FU and combination groups showed major differences (~15 to 30% decrease) in M2 TAM recruitment ($p<0.0001$ for both groups). On day twelve, major differences were observed in the anti-CCL2 (a decrease of ~20%) ($p<0.0001$) and 5-FU (a decrease of ~20%) ($p<0.0001$) groups with the combination group showing the greatest difference (a decrease of ~35%) ($p<0.0001$). The anti-CCL2 showed an ~10% decrease in M2 TAM recruitment from day three to twelve. The 5-FU group showed an ~15% decrease in M2 TAM recruitment from day three to twelve. Finally, the combination group showed an ~10% decrease in M2 TAM recruitment from day three to twelve. Overall, results show that the addition of anti-CCL2 to 5-FU shows a significant decrease in M2 TAM recruitment into the microenvironment.

Lastly, we examined the ratio of the number of M2 to total TAMs being recruited into the tumor. The control groups showed the highest M2/pan-TAM ratio at ~0.6 (Fig. 4E). This ratio remained approximately the same for the anti-CCL2 for both days (~0.5) while the 5-FU group showing a slight decrease (~0.4 to 0.35) and the combination group showing the lowest ratio (~0.18 to ~0.15). After three days, the anti-CCL2 showed a slight difference compared to the saline control ($p=0.01$) with the 5-FU showing a significant difference ($p=0.0015$) and

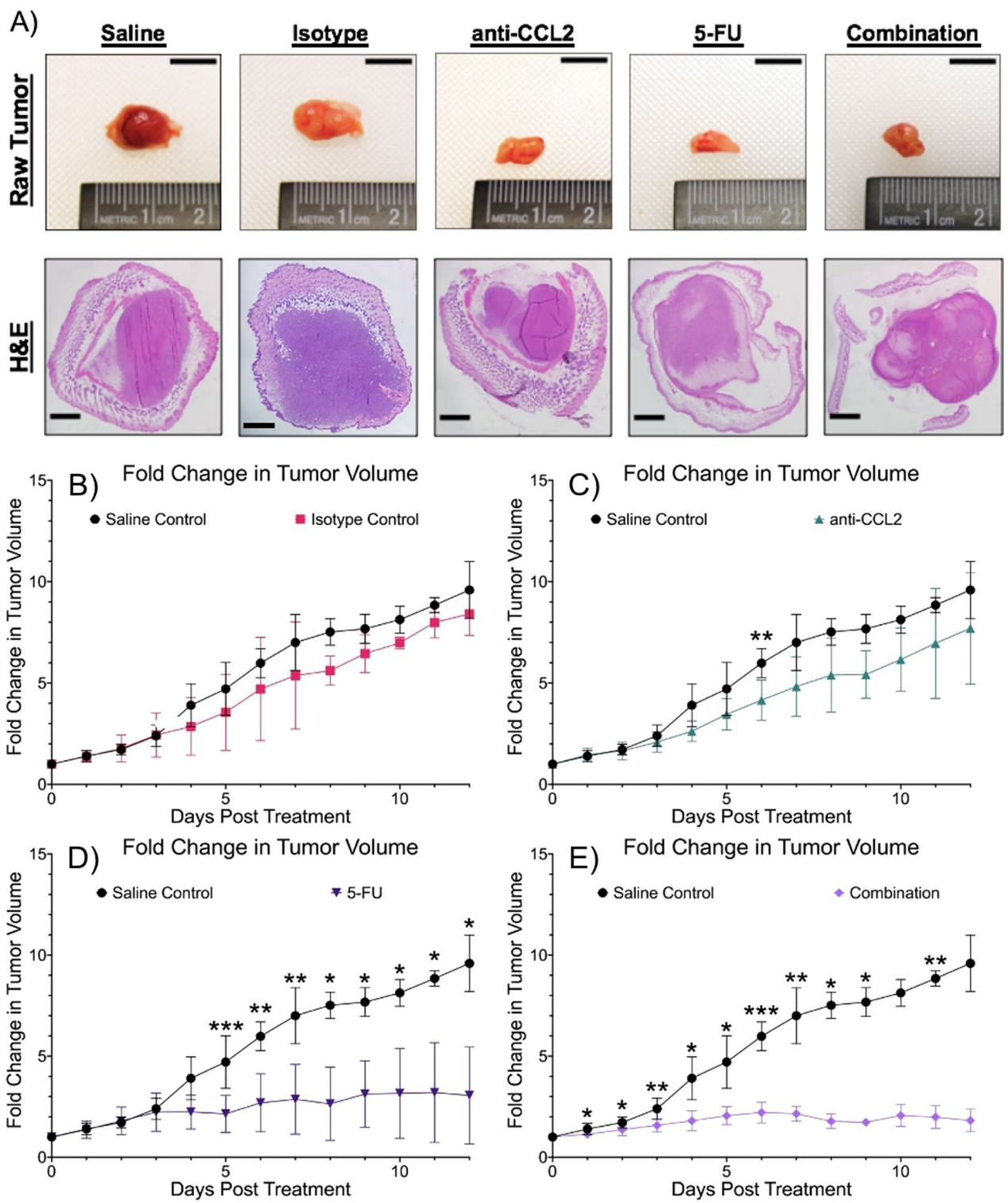

Fig. 3 Combination therapy shows slowed tumor growth. **A** Raw tumors after resection (scale bars are 10 mm) and representative H&E images (4.0X objective, 0.25NA scale bars are 100 µm). **B**–**E** Longitudinal comparisons of fold changes in tumor volume of a twelve-day duration. A mixed effects model was used to calculate statistical differences (Saline vs Combination: $*p \leq 0.05$, $**p \leq 0.01$, $***p \leq 0.001$, $****p \leq 0.0001$. Plots created in Prism (GraphPad)

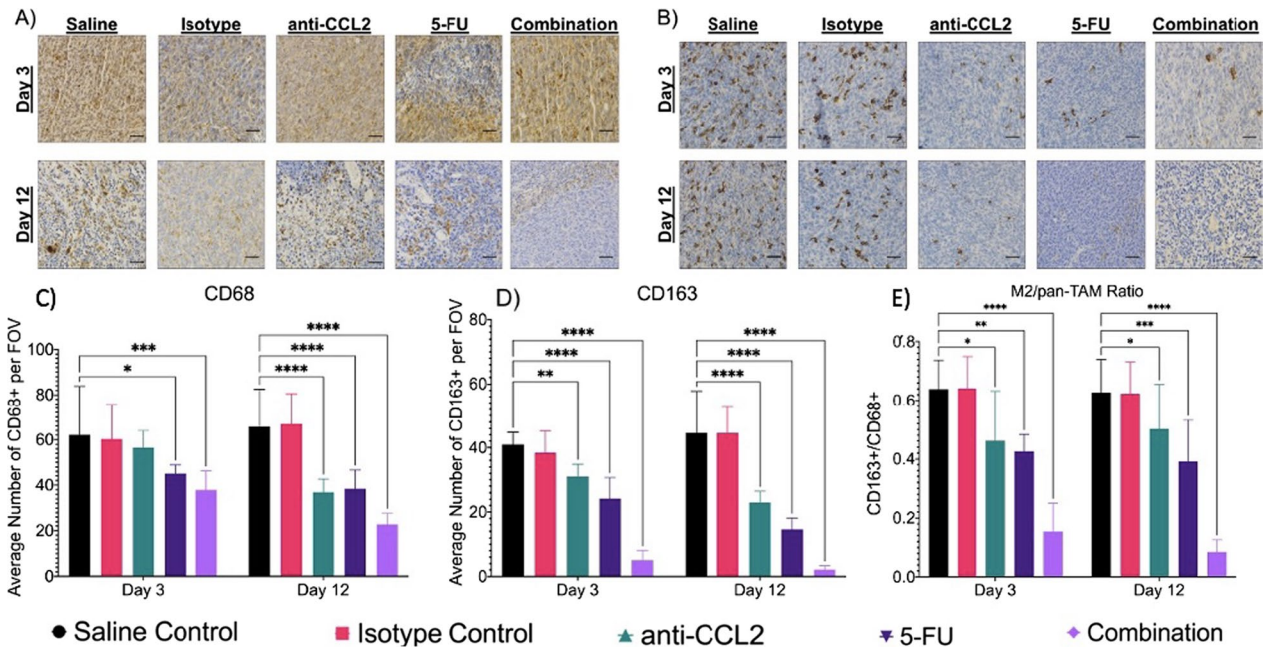

Fig. 4 Combination therapy shows decrease in total and M2 macrophage recruitment. **A** Total TAM recruitment through IHC quantification using CD68 (40X, scale bars are 20 µm). **B** M2 TAM recruitment through IHC quantification using CD163. The average number of positively stained **C** CD68 (n = 27 FOVs per group) and **D** CD163 (n = 27 FOVs per group). TAMs were counted per FOV. Then the **E** ratio of M2 TAMs to total TAMs was calculated. A mixed effects model was used to calculate statistical differences (*$p \leq 0.05$, **$p \leq 0.01$, ***$p \leq 0.001$, ****$p \leq 0.0001$). Plots created in Prism (GraphPad)

the combination group showing the greatest difference ($p < 0.0001$). Similar results are observed on day twelve ($p = 0.0462$, $p = 0.0004$, $p < 0.0001$, respectively). Taken together with the results shown in Fig. 4C, D, results indicate that the addition of anti-CCL2 to 5-FU decreases TAM infiltration into the tumor microenvironment including the TAM phenotype that induces pro-tumor function.

DRS-derived metrics quantify tumor response during treatment

To investigate the effects of combination or immunotherapy during the duration of treatment, we compared DRS-derived metrics oxygen saturation (StO_2), total hemoglobin content (THC), oxyhemoglobin (HbO_2), and deoxyhemoglobin (dHb) between groups.

Figure 5 shows the longitudinal comparisons in StO_2 between the treatment groups and the saline control. The isotype control (Fig. 5A) showed a comparable StO_2 level (~ 5–10%) with that of the saline control throughout the course of treatment. The anti-CCL2 group (Fig. 5B) showed no significant differences in StO_2 levels compared to the saline control. A small increase in StO_2 was observed on Days 7 through 9. The 5-FU group (Fig. 5C) also showed two significant differences in StO_2 levels when compared to the saline control even though the StO_2 levels were higher than the saline and isotype controls on Days 9 and 10 ($p = 0.0305$ and $p = 0.0391$, respectively). The combination group (Fig. 5D) showed higher StO_2 starting seven days after initial treatment. There were no significant differences in StO_2 when compared to the saline control.

Next, we compared the THC between groups (Fig. 6). The isotype group (Fig. 6A) had comparable THC levels with the saline control group throughout the course of treatment. The anti-CCL2 treated group (Fig. 6B) had consistently lower THC levels throughout the course of treatment. There were several significant differences observed in THC between the anti-CCL2 group and the saline control (Day 2, $p = 0.0041$; Day 3, $p = 0.0004$; Day 4, $p = 0.00398$; and Day 10, $p = 0.0465$). Like the anti-CCL2 group, the 5-FU group (Fig. 6C) also showed consistently lower levels of THC across the course of treatment. There were five days where the THC levels were significantly different (Day 2, $p = 0.0333$; Day 3, $p = 0.0041$; Day 4, $p = 0.0035$; Day 5, $p = 0.0203$, and Day 7, $p = 0.0109$). The combination group (Fig. 6D) showed significant differences of THC levels on Day 1 ($p = 0.0251$), Day 3 ($p = 0.0394$), and Day 4 ($p = 0.0110$).

HbO_2 was calculated using the following formula: $HbO_2 = StO_2$*THC, where StO_2 is the oxygen saturation and THC is the total hemoglobin in the tumor volume.

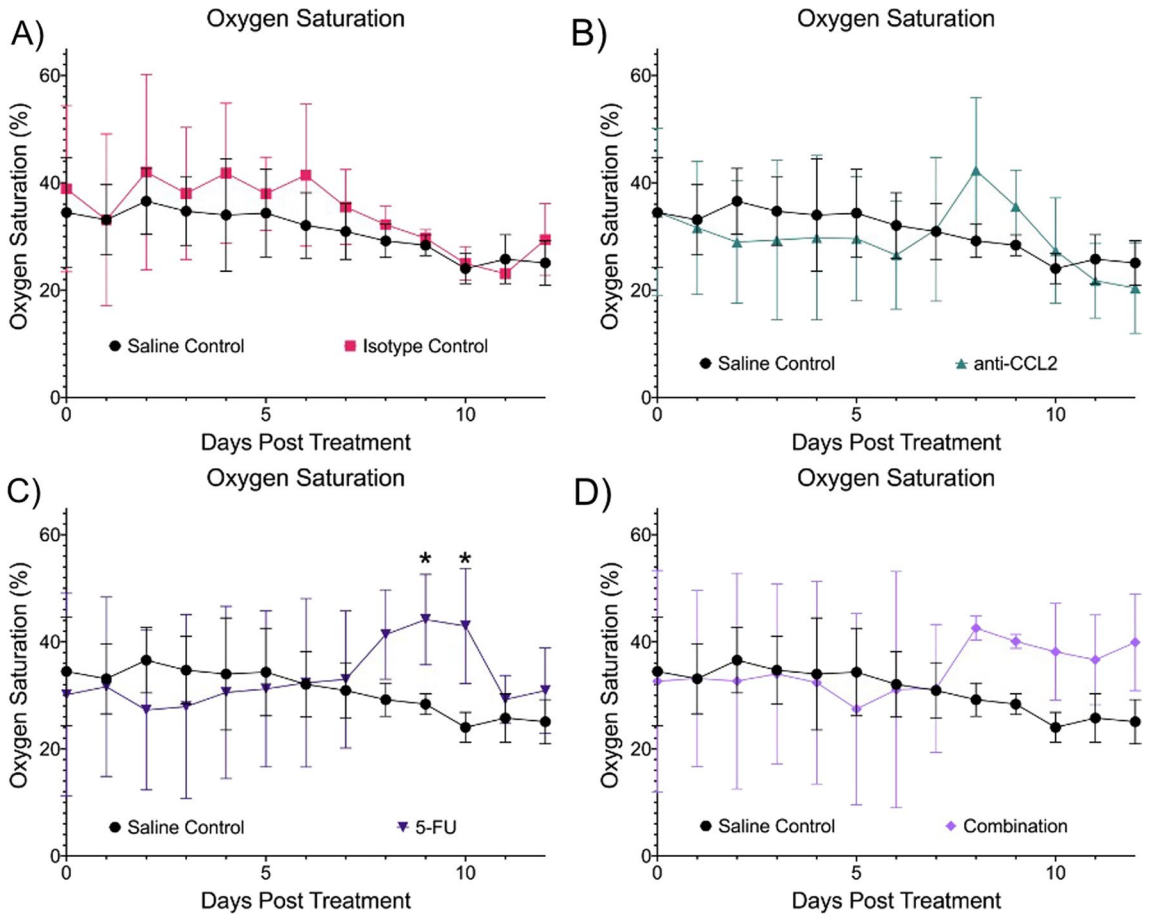

Fig. 5 Longitudinal comparisons in oxygen saturation. Each panel shows the comparison of oxygen saturation in comparison to the saline and isotype control. **A** Isotype control, **B** anti-CCL2, **C** 5-FU and **D** Combination. A mixed effects model was used to calculate statistical differences (*$p \leq 0.05$). Plots created in Prism (GraphPad)

The saline and isotype controls showed comparable levels of HbO_2 (Additional file 1: Fig. S1A). The anti-CCL2 group showed slightly lower levels of HbO_2 throughout the treatment course except for Day 8 where there was a spike in HbO_2. Significant differences were observed on Days 2 and 3 ($p = 0.0239$ and $p = 0.0467$, respectively). (Additional file 1: Fig. S1B). The 5-FU group showed varying levels of HbO_2 with increases in HbO_2 on Day 8 through 12 (Additional file 1: Fig. S1C). The combination group also showed varying levels of HbO_2 with an increase in HbO_2 after Day 8 (Additional file 1: Fig. S1D). No significant differences were observed.

Lastly, we investigated the differences in dHb (Additional file 1: Fig. S2). dHb was calculated using the following formula: $dHb = THC - HbO_2$, where THC is the total hemoglobin and HbO_2 is the oxyhemoglobin in the tumor volume. The saline and isotype controls showed similar levels of dHb across the course of treatment (Additional file 1: Fig. S2A). The anti-CCL2 treated group showed slight lower dHb levels when compared to the saline control. One difference was observed on Day 8 ($p = 0.0210$) (Additional file 1: Fig. S2B). The 5-FU and combination groups also showed consistently lower dHb levels across the treatment course. (Additional file 1: Fig. S2C and 2D). In the 5-FU group, two significant differences were observed on Days 7 through 9 ($p = 0.0049$, $p = 0.0133$, and $p = 0.0334$, respectively). One significant difference was observed on day 8 for the combination group ($p = 0.0303$).

Hypoxia expression in subcutaneous murine CRC tumors

Immunohistochemical analysis using the marker CA-IX was used to explore the differences in hypoxia between experimental groups. In Fig. 7A, representative images are shown to visually compare the amount of hypoxia in a limited tumor volume. From 9 FOVs per tumor (n = 3 per group), the hypoxic area was calculated. After three days, one major significant difference was observed.

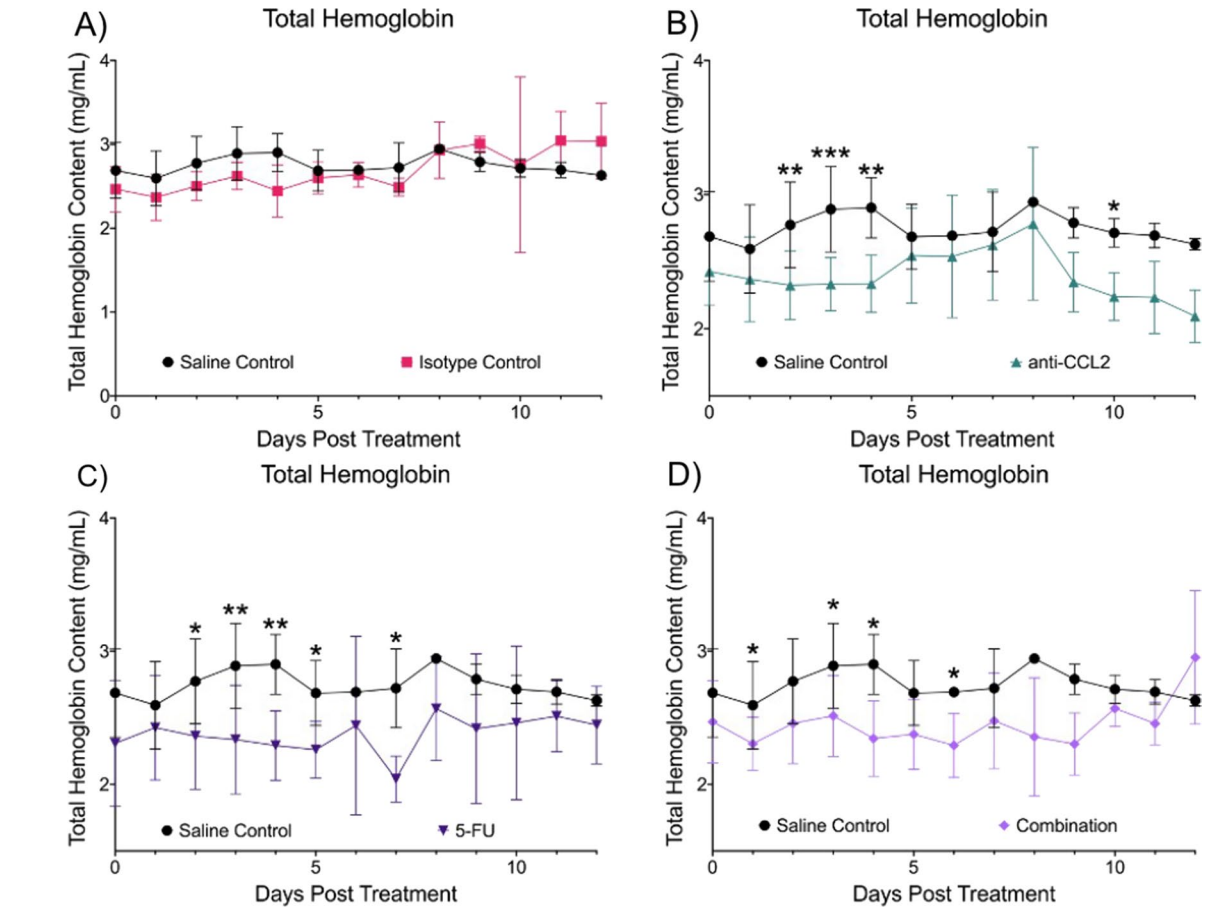

Fig. 6 Longitudinal comparisons in total hemoglobin content. Each panel shows the comparison of oxygen saturation in comparison to the saline and isotype control. **A** Isotype control, **B** anti-CCL2, **C** 5-FU and **D** Combination. A mixed effects model was used to calculate statistical differences (*$p \leq 0.05$, **$p \leq 0.01$, ***$p \leq 0.001$). Plots created in Prism (GraphPad)

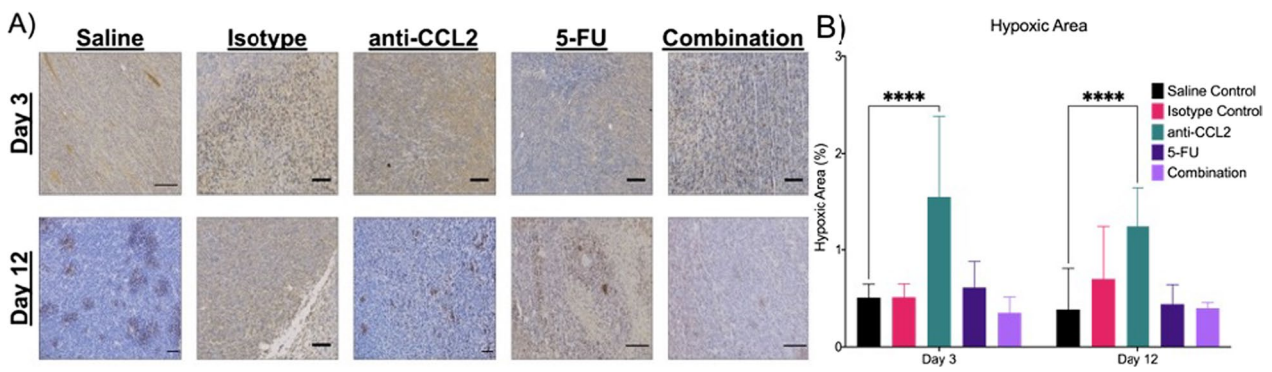

Fig. 7 The addition of anti-CCL2 to 5-FU shows a change in hypoxia. **A** Hypoxia quantification through IHC quantification using CA-IX (10X objective, 0.3NA, scale bars are 50 µm). **B** The average hypoxic area was calculated per FOV (n = 27 FOVs per group). A mixed effects model was used to calculate statistical differences. Plot created in Prism (GraphPad)

The anti-CCL2 group showed the greatest hypoxic area (~1.6%) compared to the other treatment groups, especially the saline control ($p < 0.0001$). The 5-FU group showed a slightly higher hypoxic area (~0.6%) when compared to the controls while the combination group showed a slightly lower hypoxic area (~0.4%).

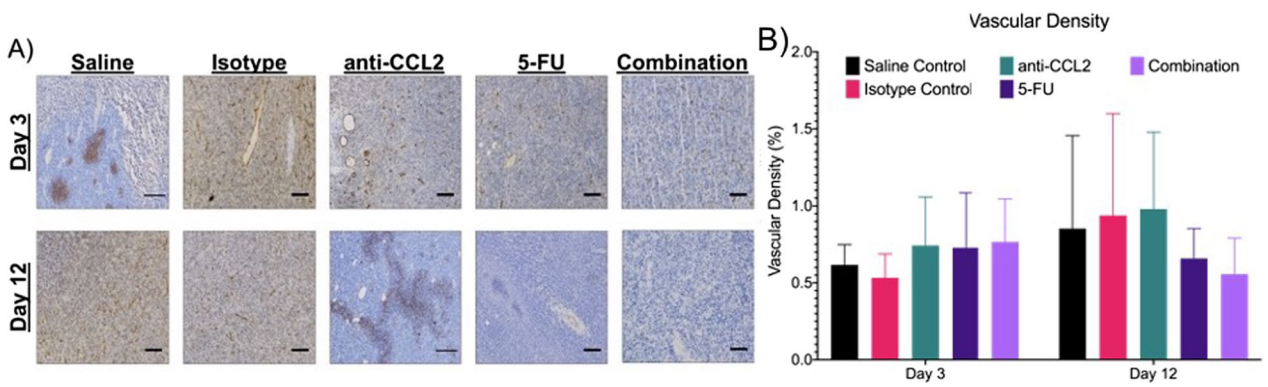

Fig. 8 The combination therapy regimen shows a decrease in new blood vessel formation. **A** Blood vessel quantification through IHC quantification using CD31 (10X objective, 0.3NA, scale bars are 50 µm). **B** The average vascular density was calculated per FOV (n = 27 FOVs per group). A mixed effects model was used to calculate statistical differences. Plot created in Prism (GraphPad)

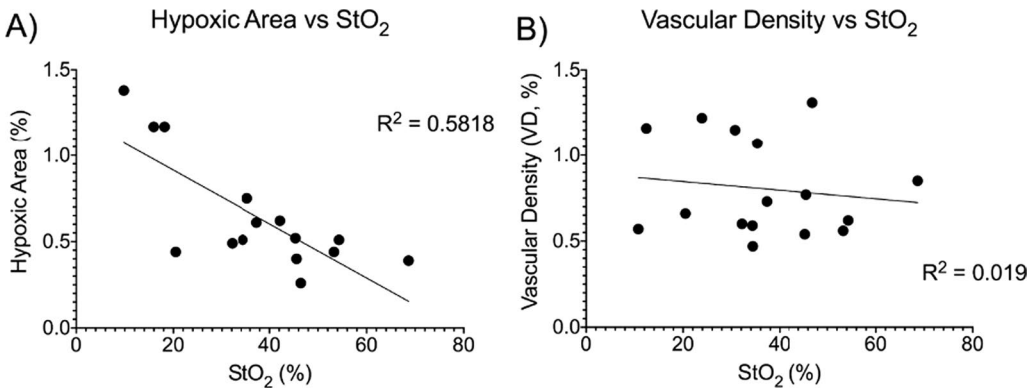

Fig. 9 Hypoxic area shows a moderate negative correlation to DRS-derived tumor oxygenation. Correlations comparing DRS-derived tumor oxygenation to **A** hypoxic area and **B** vascular density. A simple linear regression was performed to produce a goodness of fit (R^2). Plots created in Prism (GraphPad)

After twelve days, the anti-CCL2 still shows the highest hypoxic area of the treatment groups (~1.25%), but the isotype group does show an increase of ~0.5% in the hypoxic area compared to day three. Significant differences were observed in the anti-CCL2 ($p < 0.0001$) compared to the saline control on Days 3 and 12. The 5-FU group showed a slightly higher hypoxic area (~0.6%) when compared to the saline control on Day 3. Based on these results, the hypoxic area of localized tumors in the combination group was lower than that of the anti-CCL2 and 5-FU groups after three days of treatment and remains comparable to that of the 5-FU group after twelve days of treatment.

Changes in vascular density in subcutaneous murine CRC tumors

Immunohistochemical analysis using the marker CD31 was used to explore the differences in vascular density between groups. In Fig. 8A, representative images are shown to visually compare the amount of hypoxia in a limited tumor volume. From 9 FOVs per tumor (n = 3 per group), the hypoxic area was calculated. After three days of treatment, the anti-CCL2, 5-FU and combination groups also showed a higher density of blood vessels, but only a slight increase (~0.25%) compared to the saline control. After twelve days, the saline and isotype control groups along with the anti-CCL2 group showed an increase in microvasculature (~0.3 to 0.4%) while the 5-FU and combination treatment showed a decrease (~0.2%). The combination group showed the greatest decrease in the density of blood vessels on day twelve.

Validation of DRS metrics through IHC correlations

Since DRS is a new minimally invasive tool to monitor treatment response, we wanted to see if there was a correlation between the DRS-derived metrics and a trusted

immunohistochemistry marker. In Fig. 9, correlation plots were created to investigate the relationship between DRS-derived oxygenation and hypoxic area (Fig. 9A) and vascular density (Fig. 9B). There is a moderate negative correlation between hypoxic area and oxygenation, as shown in Fig. 9A ($R^2 = 0.5818$). This indicates that the higher the hypoxic area, the lower the oxygenation, which is consistent with the literature. In Fig. 9B, there is a weak correlation between vascular density and oxygenation. The correlation between hypoxic area and oxygenation shows that DRS can be used to monitor treatment response.

Discussion

Before advancements in cancer detection and treatment, conventional treatment options for locally advanced CRC include adjuvant and neoadjuvant chemotherapy and radiotherapy. Although these treatment regimens have been shown to decrease tumor burden, high recurrence rates are still a major limitation [25]. In recent years, immunotherapy strategies have shown promise in the reduction of the high recurrence rate while minimizing undesirable side effects. Various clinical trials that target vascular endothelial growth factors (VEGFs) or epidermal growth factors (EGFs) in several cancer types such as breast cancer have shown clinical success [25]. In CRC, the overall survival benefit is limited [25]. Here, we used chemokine neutralization via the CCL2 pathway to target circulating monocytes that differentiate into M2 pro-tumor TAMs.

Chemokines are involved in inducing cellular chemotaxis, making them an attractive target for CRC therapy [25]. One pathway that is involved is the CCL2 pathway. CRC recruits circulating monocytes through the release of CCL2. In the tumor microenvironment, these monocytes differentiate into tumor-associated macrophages (TAMs), which have a pervasive effect on immune cells in the microenvironment. TAMs have both anti-tumor and pro-tumor functions depending on their polarization. M2-polarized TAMs (pro-tumor) functions include immunosuppression, angiogenesis, tumor growth, increased vascular permeability, and metastatic risk [38]. Targeting of CCL2 to reduce M2-polarized TAMs is an attractive strategy in pre-clinical settings. In this study, we investigated the downstream effects of CCL2. Even though there were no significant differences in the change in tumor volume after three days, there were significant changes twelve days after the start of treatment. The blockade of CCL2 alone showed a slowing in the overall fold change in tumor volume (~threefold) compared to a saline control twelve days after the initiation of treatment. However, when anti-CCL2 was added to the gold standard 5-FU, the overall fold change in tumor growth decreased significantly (~sevenfold) compared to a saline control twelve days post-treatment. The blockade of CCL2 also showed a significant decrease in the number of TAMs recruited into the tumor microenvironment. This shows that CCL2-neutralizing immunotherapy can play an important role in early-stage CRC treatment.

Tumor oxygenation and angiogenesis have been widely studied and have been shown to have an effect on patient prognosis. Angiogenesis favors tumor growth and metastasis, while hypoxia promotes resistance to chemotherapy [38]. Tumor cells are able to adapt to hypoxic conditions through the stabilization of hypoxia-inducible transcription factor (HIF-1α), which leads to the upregulation of several genes involved in cellular proliferation and angiogenesis. One of these genes includes carbonic anhydrase (CA-IX). As mentioned in Korkeila et al. [38], patients with hypoxic tumors had poorer disease outcomes. Preoperative treatment that has slowed tumor growth can also show an increase in tumor oxygenation. Hence, preoperative therapy may reduce tumor hypoxia and therefore reduce CA-IX expression [38]. In this study, we used CA-IX to study hypoxia expression and CD31 to study vessel density after treatment with immunomodulation therapy. Alone and in combination with 5-FU, the blockade of CCL2 did show a decrease in the overall expression of CA-IX. After twelve days, the combination group showed the greatest decrease in vessel density when compared to a control. When comparing the hypoxic areas and vessel densities of the anti-CCL2 group, we found that hypoxic areas increased in a statistically significant manner (Fig. 7), while CD-31 reported blood vessel density slightly increased in a non-statistically significant manner (Fig. 8). This could be contributed to the following confounding factors: (1) during image acquisition, we may have selected a focal region of interest with aberrant vessel density (as shown in a representative image in Fig. 8A) and (2) low sensitivity of anti-CD31 staining with respect to new vessel development. CA-IX and CD31 are considered the gold standards when using immunohistochemical techniques to study tissue hypoxia and vessel formation, which allows us to examine the endpoint changes in hypoxia and vessel density [39]. However, it does not allow us to study longitudinal changes in oxygen saturation during and after the course of treatment. These markers may also not be sensitive enough to capture the small changes in hypoxia and vasculature during treatment [40]."This limitation has led many researchers to use optical techniques to non-invasively study the tumor microenvironment.

New optical techniques like diffuse reflectance spectroscopy (DRS) have been developed to study the tumor microenvironment over time. Other work has used spectroscopy techniques (near-infrared (NIR) spectroscopy) to study

tumor optical properties like oxygen saturation and total hemoglobin, in addition to lipid and water content [41]. This work shows that during the course of treatment, the addition of a CCL2 blockade to 5-FU does slightly improve tissue-derived metrics when compared to a control vehicle. 5-FU alone showed improvement in oxygen saturation and oxyhemoglobin, while anti-CCL2 only showed no significant improvements in any of the DRS metrics. For the last result section (comparisons between IHC and DRS), we wanted to use a correlation plot to determine if our DRS modality is comparable to the golden standard of IHC work. Based on our results, we observed that there is a correlation between the CA-IX hypoxic calculations and the oxygen saturation that is obtained from DRS, which could indicate that DRS could be used to monitor tumor oxygen saturation during treatment. For vessel density, we observed no clear correlation between vessel density and oxygen saturation. Future work would include creating a new optical modality that can image blood vessels to determine vessel density and be a better predictor of tumor oxygenation. Overall, our results indicate that DRS may be a useful tool in monitoring early-tumor therapeutic responses in CRC. However, due to limited penetration depth, a fixed study area, and the addition of the skin layer, the accuracy of these metrics is limited since the whole tumor could not be measured. Additionally, single-modal DRS may be limited in providing clinicians relevant information which suggests that DRS should be combined with other endoscopically compatible imaging or spectroscopic methods.

The findings in this work suggest that the blockade of CCL2 is sufficient in the reduction of TAMs that are recruited into the tumor microenvironment and has the ability to modestly alter tumor perfusion during early-tumor response to treatment even though the overall benefit is relatively modest. These findings also suggest that DRS can be a valid tool to monitor physiological changes in a subcutaneous tumor during and even after a course of treatment. Even though our results did indicate some statistical differences in the DRS and IHC data, the utility of this approach may be limited for longitudinal monitoring of a subcutaneous tumor due to the tumor volume is larger than that of the optical probe used. Future studies using a chemically-induced orthotopic model of colon cancer using anti-CCL2 in combination with 5-FU while using DRS to monitor treatment response can provide clinicians more clinically relevant evidence of using cytokine-targeted therapy in CRC.

Abbreviations

5-FU: 5-Fluorouracil; CA-IX: Carbonic anhydrase-IX; CCL2: Macrophage chemoattractant protein-1; CRC: Colorectal cancer; CRT: Chemoradiotherapy; DRS: Diffuse reflectance spectroscopy; GF: Growth factors; IHC: Immunohistochemistry; MMPs: Matrix metalloproteases; pCR: Pathologic complete response; SDS: Source detection separations; StO_2: Tissue oxygen saturation; TAMs: Tumor associated macrophages; THC: Tissue hemoglobin content; TME: Total mesorectal excision surgery; VEGF: Vascular endothelial growth factor.

Supplementary Information

The online version contains supplementary material available at https://doi.org/10.1186/s12865-022-00493-5.

Additional file 1: Longitudinal comparisons of DRS-derived oxyhemoglobin and deoxyhemoglobin.

Acknowledgements

The authors would like to thank IHC World, LLC for their technical assistance on immunohistochemistry development. Any opinions, findings, and conclusions or recommendations expressed in this material are those of the authors and do not necessarily reflect the views of the acknowledged funding agencies.

Author contributions

TJM supervised the study. GJG, NR, and TJM designed the DRS setup. SNB, GJG, and TJM designed the experiments. SNB and GJG performed the experiments. SNB analyzed the data. SNB and GJG wrote the manuscript. All authors read and approved the final manuscript.

Funding

This material is based on work supported by the National Science Foundation (CBET 1751554) and the Arkansas Biosciences Institute.

Availability of data and materials

The authors declare that all data supporting the findings of this study are available within the article and its supplementary information files. A public repository of our datasets can be found in this FigShare link: https://figshare.com/projects/TAM_Study_-_Raw_Files/131684

Declarations

Ethics approval and consent to participate

All animal procedures were approved by the University of Arkansas (IACUC #18060 and #21014). All methods were performed in accordance with the relevant guidelines and regulations. All animal experiments met the ARRIVE guidelines.

Consent for publication

Not applicable.

Competing interests

The authors declare that they have no competing interests.

Received: 9 December 2021 Accepted: 6 April 2022
Published online: 23 April 2022

References

1. Siegel RL, Miller KD, Fuchs H, Jemal A. Cancer statistics. CA Cancer J Clin. 2021;71(1):7–33.
2. Ferrari L, Fichera A. Neoadjuvant chemoradiation therapy and pathological complete response in rectal cancer. Gastroenterol Rep. 2015;3:277–88.
3. Dienstmann R, Villacampa G, Sveen A, Mason MJ, Niedzwiecki D, Nesbakken A, et al. Relative contribution of clinicopathological variables, genomic markers, transcriptomic subtyping and microenvironment features for outcome prediction in stage II/III colorectal cancer. Ann Oncol. 2019;30:1622–9.
4. Landmann RG, Weiser MR. Surgical management of locally advanced and locally recurrent colon cancer. Clin Colon Rectal Surg. 2005;18:182–9.
5. Boland PM, Fakih M. The emerging role of neoadjuvant chemotherapy for rectal cancer. J Gastrointest Oncol. 2014;5:362–73.

6. Lynch D, Murphy A. The emerging role of immunotherapy in colorectal cancer. Ann Transl Med. 2016;4:16.
7. Yuan J, Hegde PS, Clynes R, Foukas PG, Harari A, Kleen TO, et al. Novel technologies and emerging biomarkers for personalized cancer immunotherapy. J Immunother Cancer. 2016;4:3.
8. Sanchez-Castanon M, Bujanda L, Herreros-Villanueva M. Immunotherapy in colorectal cancer: what have we learned so far? Europe PMC. 2016;5:11–24.
9. Chun E, Lavoie S, Michaud M, Gallini CA, Kim J, Soucy G, et al. CCL2 Promotes colorectal carcinogenesis by enhancing polymorphonuclear myeloid-derived suppressor cell population and function. Cell Rep. 2015;12:244–57.
10. Erreni M, Mantovani A, Allavena P. Tumor-associated Macrophages (TAM) and inflammation in colorectal cancer. Cancer Microenviron. 2011;4:141–54.
11. Li M, Li M, Yin T, Shi H, Wen Y, Zhang B, et al. Targeting of cancer-associated fibroblasts enhances the efficacy of cancer chemotherapy by regulating the tumor microenvironment. Mol Med Rep. 2016;13:2476–84.
12. Guo Q, Jin Z, Yuan Y, Liu R, Xu T, Wei H, et al. New Mechanisms of tumor-associated macrophages on promoting tumor progression: recent research advances and potential targets for tumor immunotherapy. J Immunol Res. 2016;1:5.
13. Zhang X, Chen Y, Hao L, Hou A, Chen X, Li Y, et al. Macrophages induce resistance to 5-fluorouracil chemotherapy in colorectal cancer through the release of putrescine. Cancer Lett. 2016;381:305–12.
14. Kaler P, Godasi BN, Augenlicht L, Klampfer L. The NF-κB/AKT-dependent induction of Wnt signaling in colon cancer cells by macrophages and IL-1β. Cancer Microenviron. 2009;2:69–80.
15. Popovic ZV, Sandhoff R, Sijmonsma TP, Kaden S, Jennemann R, Kiss E, et al. Sulfated glycosphingolipid as mediator of phagocytosis: SM4s enhances apoptotic cell clearance and modulates macrophage activity. J Immunol (Baltimore, Md:1950). 2007;179:6770–2.
16. Herbeuval J-P, Lelievre E, Lambert C, Dy M, Genin C. Recruitment of STAT3 for production of IL-10 by colon carcinoma cells induced by macrophage-derived IL-6. J Immunol (Baltimore, Md:1950). 2004;172:4630–2.
17. Guo C, Buranych A, Sarkar D, Fisher PB, Wang X-Y. The role of tumor-associated macrophages in tumor vascularization. Vasc Cell. 2013;5:20.
18. Zou K, Wang Y, Hu Y, Zheng L, Xu W, Li G. Specific tumor-derived CCL2 mediated by pyruvate kinase M2 in colorectal cancer cells contributes to macrophage recruitment in tumor microenvironment. Tumour Biol J Int Soc Oncodev Biol Med. 2017;39:10.
19. Barbera-Guillem E, Nyhus JK, Wolford CC, Friece CR, Sampsel JW. Vascular endothelial growth factor secretion by tumor-infiltrating macrophages essentially supports tumor angiogenesis, and IgG immune complexes potentiate the process. Cancer Res. 2002;62:7042–9.
20. Fuanda Y, Noguchi T, Kikuchi R, Takeno S, Uchida Y, Gabbert HE. Prognostic significance of CD8+ T cell and macrophage peritumoral infiltration in colorectal cancer. Oncol Rep. 2003;10:309–13.
21. Sugita J, Ohtani H, Mizoi T, Saito K, Shiiba K, Sasaki I, et al. Close association between Fas ligand (FasL; CD95L)-positive tumor-associated macrophages and apoptotic cancer cells along invasive margin of colorectal carcinoma: a proposal on tumor-host interactions. Jpn J Cancer Res. 2002;93:320–8.
22. Forssell J, Oberg A, Henriksson ML, Stenling R, Jung A, Palmqvist R. High macrophage infiltration along the tumor front correlates with improved survival in colon cancer. Clin Cancer Res. 2007;13:1472–9.
23. Zhou Q, Peng R-Q, Wu X-J, Xia Q, Hou J-H, Ding Y, et al. The density of macrophages in the invasive front is inversely correlated to liver metastasis in colon cancer. J Transl Med. 2010;8:13.
24. Burmeister K, Quagliata L, Andreozzi M, Eppenberger-Castori S, Matter MS, Perrina V, et al. Vascular endothelial growth factor A amplification in colorectal cancer is associated with reduced M1 and M2 macrophages and diminished PD-1-expressing lymphocytes. PLoS ONE. 2017;1:5.
25. Bess SN, Greening GJ, Muldoon TJ. Efficacy and clinical monitoring strategies for immune checkpoint inhibitors and targeted cytokine immunotherapy for locally advanced and metastatic colorectal cancer. Cytokine Growth Factor Rev. 2019;49:1–9.
26. McClellan JL, Davis JM, Steiner JL, Enos RT, Jung SH, Carson JA, et al. Linking tumor-associated macrophages, inflammation, and intestinal tumorigenesis: role of MCP-1. Am J Physiol. 2012;303:G1087–95.
27. Popivanova BK, Kostadinova FI, Furuichi K, Shamekh MM, Kondo T, Wada T, et al. Blockade of a chemokine, CCL2, reduces chronic colitis-associated carcinogenesis in mice. Cancer Res. 2009;69:7884–92.
28. Zhu X, Fujita M, Snyder LA, Okada H. Systemic delivery of neutralizing antibody targeting CCL2 for glioma therapy. J Neuro-Oncol. 2011;104:83–92.
29. Svensson S, Abrahamsson A, Rodriguez GV, Olsson A-K, Jensen L, Cao Y, et al. CCL2 and CCL5 are novel therapeutic targets for estrogen-dependent breast cancer. Clin Cancer Res. 2015;21:3794–805.
30. Kirk PS, Koreckij T, Nguyen HM, Brown LG, Snyder LA, Vessella RL, et al. Inhibition of CCL2 signaling in combination with docetaxel treatment has profound inhibitory effects on prostate cancer growth in bone. Int J Mol Sci. 2013;14:10483–96.
31. Singh M, Khong H, Dai Z, Huang X-F, Wargo JA, Cooper ZA, et al. Effective innate and adaptive antimelanoma immunity through localized TLR7/8 activation. J Immunol (Baltimore, Md:1950). 2014;193:4722–31.
32. Wu Y, Deng Z, Wang H, Ma W, Zhou C, Zhang S. Repeated cycles of 5-fluorouracil chemotherapy impaired anti-tumor functions of cytotoxic T cells in a CT26 tumor-bearing mouse model. BMC Immunol. 2016;17:29.
33. Palframan RT, Jung S, Cheng G, Weninger W, Luo Y, Dorf M, et al. Inflammatory chemokine transport and presentation in HEV: a remote control mechanism for monocyte recruitment to lymph nodes in inflamed tissues. J Exp Med. 2001;194:1361–73.
34. Rajaram N, Gopal A, Zhang X, Tunnell JW. Experimental validation of the effects of microvasculature pigment packaging on in vivo diffuse reflectance spectroscopy. Wiley Online Library. 2010;42:680–8.
35. Prahl S. Optical Absorption of Hemoglobin. [cited 2021Mar17]. Available from: https://omlc.org/spectra/hemoglobin/
36. Greening GJ, James HM, Dierks MK, Vongkittiargorn N, Osterholm SM, Rajaram N, et al. Towards monitoring dysplastic progression in the oral cavity using a hybrid fiber-bundle imaging and spectroscopy probe. Nat News. 2016;6:26.
37. Greening GJ, James HM, Powless AJ, Hutcheson JA, Dierks MK, Rajaram N, et al. Fiber-bundle microendoscopy with sub-diffuse reflectance spectroscopy and intensity mapping for multimodal optical biopsy of stratified epithelium. Biomed Opt Express. 2015;6:4934–50.
38. Korkeila E, Talvinen K, Jaakkola P, Minn H, Syrjänen K, Sundström J, et al. Expression of carbonic anhydrase IX suggests poor outcome in rectal cancer. Br J Cancer. 2009;100:874–80.
39. Dewhirst MW, et al. Rationale for hypoxia assessment and amelioration for precision therapy and immunotherapy studies. J Clin Investig. 2019;129(2):489–91. https://doi.org/10.1172/JCI126044.
40. Matsuda Y, Hagio M, Ishiwata T. Nestin: a novel angiogenesis marker and possible target for tumor angiogenesis. World J Gastroenterol. 2013;19(1):42–8. https://doi.org/10.3748/wjg.v19.i1.42.
41. Elfarnawany MH. Signal processing methods for quantitative power doppler microvascular angiography. Electronic Thesis and Dissertation Repository 3106 (2015).

Publisher's Note